ORIGINAL RESEARCH

Seismic Retrofitting of Flat Adobe Vaults in Historic Iranian Windcatchers Using Steel and FRP Bars: A Nonlinear Time-History Analysis Approach for Heritage Conservation

Shahraki M. [1*] **Agha Kasiri sh** [2]

Abstract:

The historic windcatcher structures (Āsbaads) of Qal'eh Machi in Sistan, Iran, exemplify the ingenuity of vernacular earthen construction in arid regions. Their flat adobe vaults, central to both structural form and passive cooling function, are increasingly threatened by seismic vulnerability and environmental degradation. Traditional retrofitting methods—such as external bracing or massive overlays—have often proven inadequate, not only due to their intrusive nature but also because they can alter the architectural identity and impose additional loads on the fragile adobe substrate. To address these limitations, this study investigates the use of Near-Surface Mounted (NSM) Fiber-Reinforced Polymer (FRP) bars as a modern seismic retrofitting solution. FRP systems offer several engineering advantages, including light weight, high tensile strength, and excellent durability against corrosion and moisture, making them highly compatible with adobe structures. The research employs nonlinear dynamic time-history analyses using calibrated finite element models in ABAQUS 2020, applying three real earthquake records (Sarpol-e Zahab, Tabas, and Northridge) representing both near- and far-field ground motions. Findings demonstrate that FRP retrofitting reduces peak displacement and plastic strain by up to 54% and 48%, respectively, while also achieving up to 52% reduction in base shear. Compared to steel reinforcement, FRP systems consistently deliver better ductility, lower stiffness degradation, and greater energy dissipation under seismic loading. These results confirm that NSM-FRP retrofitting provides a structurally effective and minimally invasive strategy for protecting flat adobe vaults without compromising their architectural authenticity. This study contributes to the field of heritage conservation engineering by validating a performance-based retrofitting framework that is context-sensitive, technically robust, and culturally appropriate for safeguarding traditional earthen architecture in earthquake-prone regions.

Keywords:
Retrofitting; FRP parts; Flat adobe vault; Heritage conservation; Nonlinear time-history analysis

✉*Corresponding author Email: Mehdi.shahraki@iau.ac.ir
1. Department of Civil Engineering, Zah.C., Islamic Azad University, Zahedan, Iran
2. Department of Civil Engineering, TS.C., Islamic Azad University, Tehran, Iran. Sh.aghakasiri@aiu.ir

1. Introduction

The historical windcatcher structures (Āsbaads) of the Sistan region in southeastern Iran represent an exceptional example of vernacular architecture that seamlessly integrates passive cooling techniques with socio-economic functions such as grain milling and food storage [1]. Among these structures, the flat adobe vaults—horizontal load-bearing elements spanning the windcatcher chambers—are particularly noteworthy due to their unique geometric configuration and material composition. These vaults reflect a centuries-old adaptation to arid climatic conditions and have become emblematic of Iranian desert architecture [2].

Over time, however, environmental factors have significantly degraded these structures. Prolonged exposure to sulfate-rich soils, salt-laden winds, and cyclical humidity fluctuations have compromised the cohesion of adobe materials, leading to progressive deterioration. Structurally, the absence of embedded tensile reinforcement in most of these vaults, combined with their flat geometries, makes them especially vulnerable to seismic forces. This issue is particularly critical given Iran's seismicity, classified among the most earthquake-prone regions globally. Despite their cultural and architectural value, most restoration efforts have remained superficial and cosmetic, lacking the integration of engineering-based assessments and retrofitting strategies [3].

To address this vulnerability, the present study investigates the seismic behavior of flat adobe vaults in the historic windcatchers of Qal'eh Machi, Sistan. Using advanced nonlinear time-history analyses in ABAQUS 2020, we simulate the structural response of these vaults under seismic loading from Sarpol-e Zahab, Tabas, and Northridge earthquake records. Two retrofitting strategies are comparatively assessed: (1) traditional steel rebars, and (2) Near-Surface Mounted (NSM) Fiber Reinforced Polymer (FRP) bars. The objective is to provide conservation engineers with performance-based insights into how these solutions impact peak displacement, plastic strain, energy dissipation, and overall resilience.

The use of composite materials like FRP for seismic retrofitting of earthen structures has gained traction in recent years. Faggella et al. [5] conducted a comprehensive review of earthen retrofitting techniques and emphasized the superior mechanical behavior of FRP systems in heritage contexts highlighting their high strength-to-weight ratio, corrosion resistance, and compatibility with traditional materials. Their findings suggest that proper anchorage systems and confinement detailing are key to achieving long-term seismic performance.

In parallel, probabilistic evaluation frameworks have emerged as powerful tools for assessing seismic risk in heritage structures. Lu and Zhang [6] proposed a fragility-based approach incorporating Monte Carlo simulations to evaluate variability in structural response. Their framework provides critical guidance for developing resilience indices, which form a major analytical component of this study.

Dimitri and Trentinabin [4] contributed a Discrete Element Method (DEM) for evaluating the quasi-static response of unreinforced masonry arches. Their results underscore the influence of frictional interface behavior and geometric constraints considerations particularly relevant in flat adobe vaults with limited arching action. From a material durability standpoint, Toutanji and Balaguru [7] experimentally evaluated the performance of FRP- and GFRP-confined adobe walls under environmental exposure conditions. Their findings indicate that FRP systems maintain strength and ductility under variable humidity but may lose performance under freeze-thaw cycles a key consideration for retrofitting in Sistan's semi-arid climate.

In a different but complementary line of research, Garmeh et al. [8] explored the use of Self-Centering Eccentrically Braced Frames (SC-EBFs) utilizing Shape Memory Alloys (SMA). Although their study focused on steel structures, their emphasis on energy-dissipative and self-recovering mechanisms provides inspiration for adaptive retrofitting solutions in earthen heritage contexts.

Taken together, these studies provide a strong theoretical and experimental foundation, yet none have directly addressed the unique seismic behavior of flat adobe vaults within windcatcher systems. This study fills that gap through a comprehensive simulation-based investigation, calibrated material modeling, and development of seismic fragility curves and resilience metrics tailored to the heritage conservation of adobe structures.

2. Theoretical Framework

2.1. Architectural Characteristics of the Qaleh-Machi Windmills, Iran

The investigated windcatchers are located within the archaeological precinct of Hosehdar, positioned in the southeastern sector of the Qaleh-Machi fortress complex. Occupying a land parcel of approximately 3,300 square meters, the windmill ensemble is composed of modular structures, each originally covering an estimated area of 30 by 30 meters. However, detailed site measurements indicate that the actual footprint of an individual windcatcher is closer to 9.5 meters by 7 meters, yielding a total floor area of approximately 66.5 square meters per unit.

Each windmill is elevated on a platform raised 40 centimeters above the natural ground level, with a total structural elevation reaching 80.6 centimeters from the base. The roofing systems vary between flat and domed configurations, both finished with traditional mud-and-straw plaster, as depicted in Figures 1 and 2.Architecturally, all units exhibit a singular southern-facing entrance, while the surrounding walls exhibit substantial mass with a thickness of up to 1 meter. Notably, the interior spaces are devoid of ornamental detailing, emphasizing the utilitarian nature of these constructions. The primary building materials consist of sun-dried adobe blocks bound with mud-straw mortar, while kiln-fired bricks have been utilized selectively in the external floor layers. The detailed architectural layouts of the windmills are illustrated in Figures 3 and 4.

Fig. 1. Location of the adobe windcatcher structures in Āsbaads of Sistan (Iran) within the historical district of Howz-e-Dar

Fig. 2. Northern and Western Elevation Views of Windmill No. 2 After Restoration

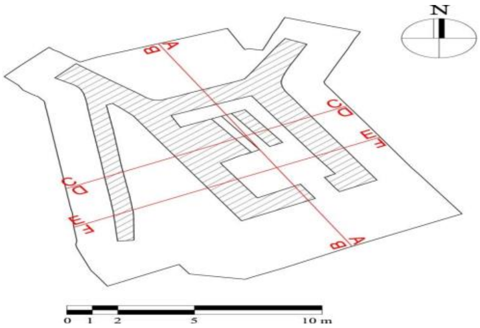

Fig. 3. Section plan of Windcatcher No. 2 at a scale of 1:200 from the base of the adobe windcatcher structures in Āsbaads of Sistan (Iran)

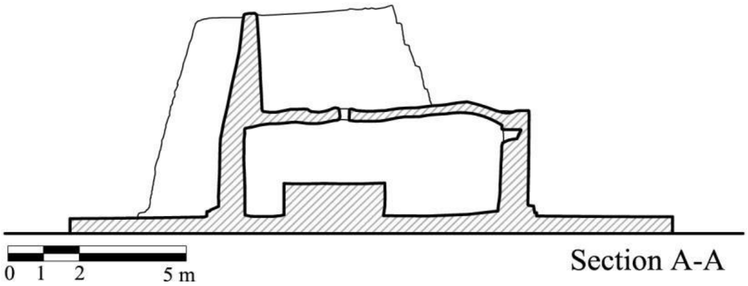

Fig. 4. Cross-section of adobe windcatcher structures in Āsbaads of Sista n (Iran) with Flat vaults arched (scale 1:200)

To accurately characterize the material behavior of the adobe and mortar used in the flat vault structures, a representative sample was extracted from an Āsbaad (traditional windmill) located in the Qal'eh Machi region of Sistan, Iran. The collected material was submitted to a certified geotechnical laboratory, where unconfined compressive strength (UCS) testing was performed in accordance with ASTM D2166 standards. The detailed results for each tested sample are compiled in Table 1.

In addition to the soil-based materials, mechanical and dimensional properties of the reinforcement systems used in this study including conventional steel rebars and Fiber Reinforced Polymer (FRP) bars are outlined in Table 2. These reinforcements were applied in different retrofitting configurations to assess their seismic performance.

A summary of the geometrical and physical attributes of the analyzed vaults, modeled under various strengthening scenarios, is presented in Table 3. These parameters were used to calibrate the numerical models and to ensure consistency with real-world construction characteristics.

Table 1. Material Properties of Mudbrick and Mortar Used in the Domed Roof of the Qaleh Machi Windmill, Iran

Sample Description 3.81 × 7.61	Elastic Modulus (E_1) (MPa)	Tensile Strength (X□) (MPa)	Compressive Strength (Xc)(MPa)	Moisture Content (%)	Failure Strain (%)
Mortar	1391	1.7	10.8	1.0	1.2
Mudbrick	1776	1.4	8.9	0.7	1.0

Table 2. Mechanical and Physical Properties of FRP and Steel Reinforcement Bars [9]

Property	FRP Rebar	Steel Rebar
Specific gravity	7.1	9.7
Yield strength (MPa)	701	600
Ultimate strength (MPa)	483	380
Compressive strength (MPa)	310 – 482	380
Tensile modulus (GPa)	55	200
Coefficient of thermal expansion	9.9	7.11

Table 3. Model Specifications Based on Geometry, Retrofitting Technique, and Earthquake Record

Model ID	Vault Geometry	Retrofitting Type	Earthquake Record	Time
F-S-1	Flat	Unretrofitted	Sarpol-e Zahab	2017
F-S-2	Flat	Retrofitted with Steel Rebar	Sarpol-e Zahab	2017
F-S-3	Flat	Retrofitted with FRP Rebar	Sarpol-e Zahab	2017
F-T-1	Flat	Unretrofitted	Tabas	1978
F-T-2	Flat	Retrofitted with Steel Rebar	Tabas	1978
F-T-3	Flat	Retrofitted with FRP Rebar	Tabas	1978
F-N-1	Flat	Unretrofitted	Northridge	1994
F-N-2	Flat	Retrofitted with Steel Rebar	Northridge	1994
F-N-3	Flat	Retrofitted with FRP Rebar	Northridge	1994

2.2. Evaluation of Earthquake Records

To conduct a nonlinear time-history analysis of the flat vault structure under investigation, a set of ground motion records was selected from both international and regional seismic events. The dataset includes two globally recognized earthquakes Northridge and Tabas as well as the Sarpol-e Zahab earthquake, a significant seismic event that occurred in western Iran. These records were obtained from the Pacific Earthquake Engineering Research Center (PEER) Ground Motion Database, ensuring reliable source integrity and standardized spectral characteristics. The selected accelerograms, depicted in Figures 5 to 7, were chosen to represent a broad range of frequency content and peak ground acceleration values, allowing for a robust dynamic assessment of the vault's seismic response.

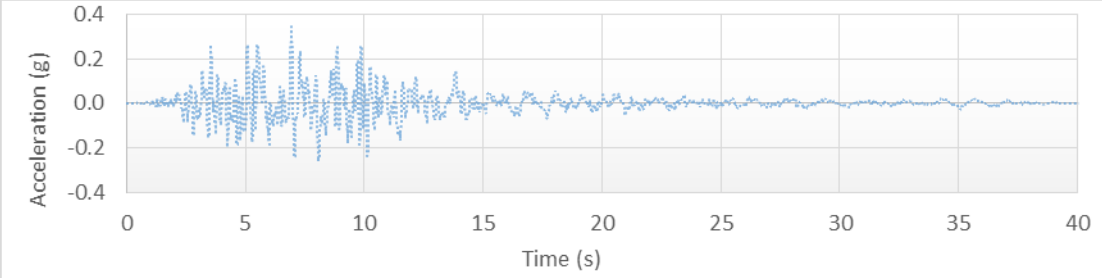

Fig. 5. The Horizontal Component of the Sarpol-e Zahab Earthquake Record (2017)

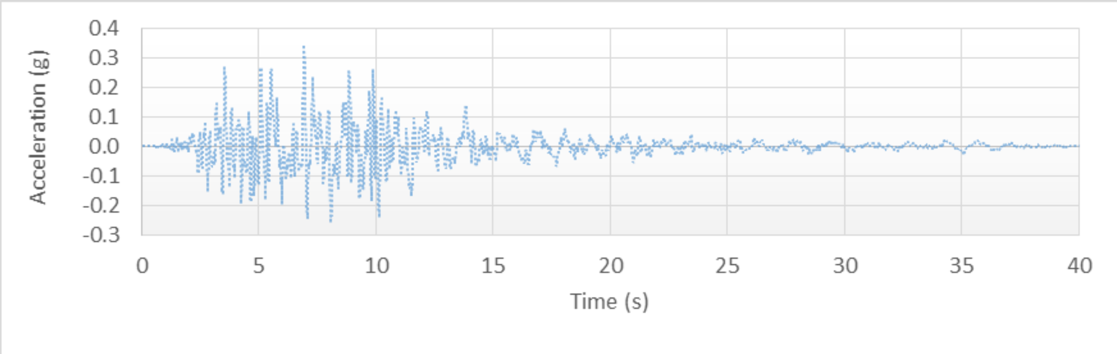

Fig. 6. The Horizontal Component of the Tabas Earthquake Record (1978)

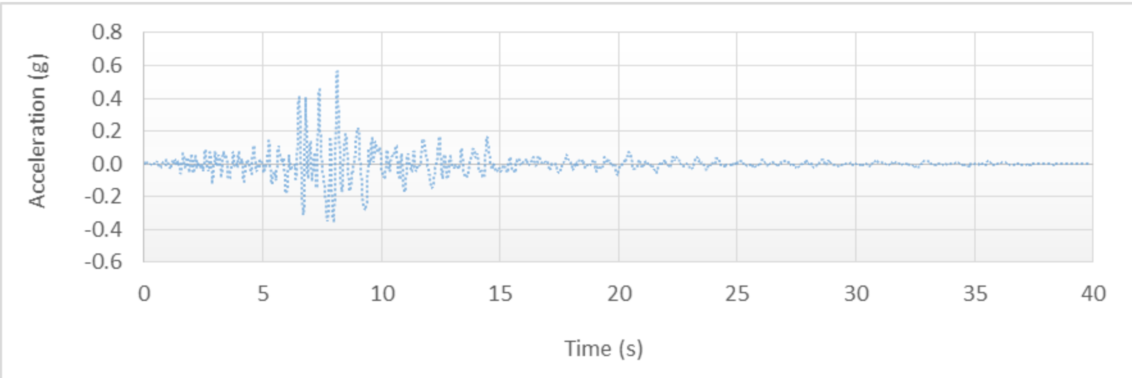

Fig. 7. The Horizontal Component of the Northridge Earthquake Record (1994)

The essential characteristics of the selected earthquake ground motion records are summarized in Table 5. As shown, the chosen records exhibit a wide spectrum of frequency content and peak acceleration levels, making them suitable for evaluating structural response under varied seismic demands. Although some of these records exceed the minimum criteria outlined in the Iranian Seismic Code (Standard No. 2800)—which stipulates that the strong-motion duration must be at least 10 seconds or three times the fundamental period of the structure, whichever is greater this selection was intentional. It aligns with the primary objective of this study, which is to examine the seismic behavior and retrofitting efficacy of a structurally deficient adobe flat vault under diverse earthquake excitations.

To ensure the consistency of input motions, the combined response spectra were computed within a target period range of 0.2T to 1.5T and compared with the code-defined design spectrum. A scale factor was derived such that the average spectral accelerations across this range consistently exceeded 1.17 times the corresponding values from the design spectrum. These scale factors were then applied to the ground motion records, and the scaled signals were subsequently imported into the time-history analysis. Figure 8 presents the combined spectra for the three selected earthquake records, as prepared for input into the numerical modeling framework.

Table 4. Characteristics of Selected Ground Motion Records

Ground Motion Record	Peak Ground Acceleration (g)	Peak Ground Velocity (cm/s)	Peak Ground Displacement (cm)
Sarpol-e Zahab	0.432	45.677	9.043
Tabas	0.854	98.949	37.527
Northridge	0.568	51.826	9.034

Table 5. Summary of the Seismic Parameters of the Selected Earthquakes

Parameter	Sarpol-e Zahab Earthquake – Iran	Tabas Earthquake – Iran	Northridge Earthquake – USA
Moment Magnitude (Mw)	7.3	7.8	7.3
Local Date and Time of Occurrence	November 12, 2017 – 21:48:16	September 16, 1978 – 15:35:56	January 17, 1994 – 12:30:55
Epicenter Longitude (°)	45.9 E	40.57 E	118.517 W
Epicenter Latitude (°)	34.84 N	35.33 N	34.312 N
Hypocentral Depth (km)	11	5	11.4

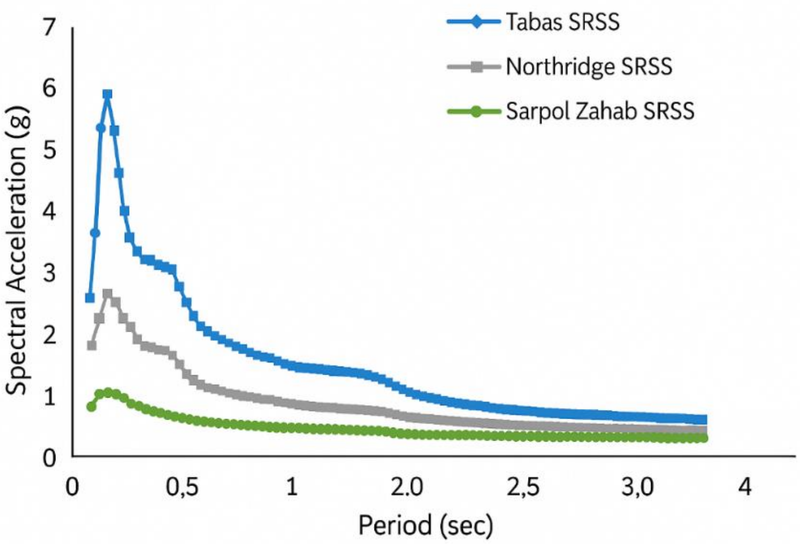

Fig. 8. Combined and Non-Directional Response Spectrum (Square Root of the Sum of Squares) of the Three Selected Earthquakes

3. Methodology

3.1. Numerical Study

A comprehensive experimental-numerical study conducted by Tighiouart et al. [9] examined the impact of seismic retrofitting on adobe masonry arch bridges. Their investigation involved testing a full-scale (1:1) stone arch prototype subjected to simultaneous vertical and lateral loads, modeled and analyzed using ABAQUS 2020, as depicted in Figure 3. Vertical loads were applied via spring elements positioned atop the imposts, followed by incremental application of lateral forces along the arch span to simulate realistic seismic actions. The first phase of the test involved evaluating the unreinforced configuration of the arch. In contrast, the second phase incorporated an external strengthening scheme using Carbon Fiber Reinforced Polymer (CFRP) laminates bonded to the extrados and intrados in areas identified as tension-critical. The onset of initial cracking in the plain model—primarily due to tensile stresses—was used to inform the CFRP placement strategy. Results indicated a substantial improvement in lateral load resistance and out-of-plane stability for the strengthened specimen. To approximate the composite mechanical behavior of the masonry comprising both stone blocks and mortar joints—an equivalent elastic modulus of 4050 MPa was adopted. The finite element mesh was constructed using reduced integration 8-node linear brick elements (C3D8R), which were consistently employed throughout the model for accurate stress distribution and computational efficiency.

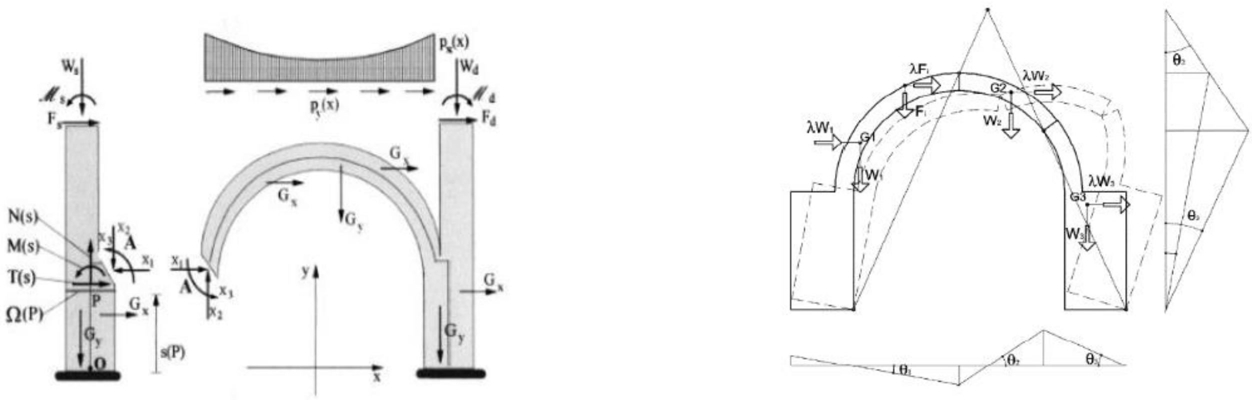

Fig. 9. Arrangements of lateral and radial anchorages in the studied bridge [9]

Figure 10 presents the numerical distribution of stress fields across the structural model. As depicted in Figures 11 and 12, the simulation outcomes achieved in the current study demonstrate a high degree of consistency with the findings from previous analytical research focused on the structural behavior of the Asbad windmill vault. This alignment substantiates the reliability and robustness of the present modeling approach [10].

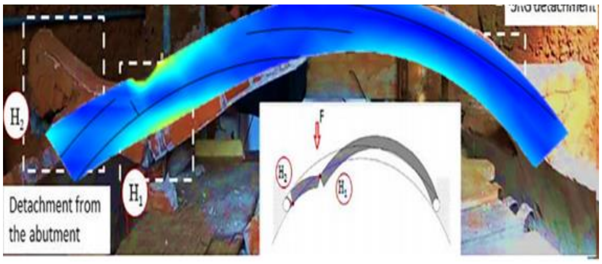

Fig. 10. Stresses in the mode validation

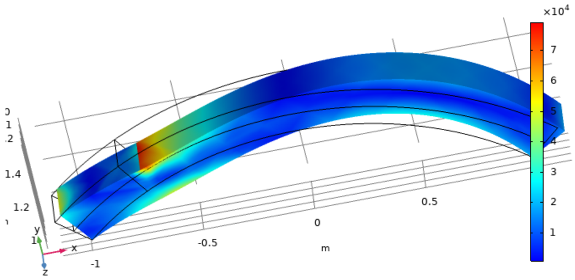

Fig. 11. Arrangement of the curve results

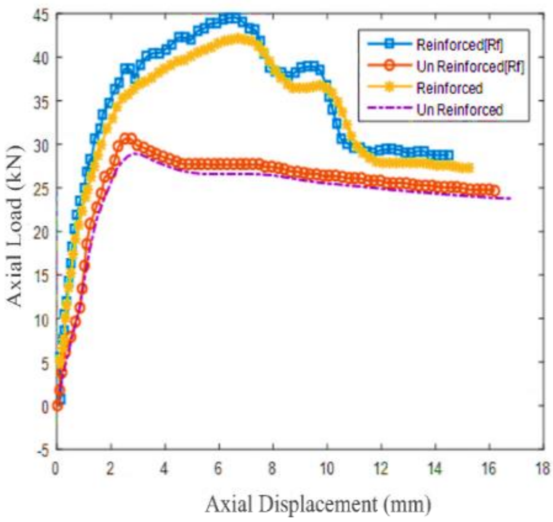

Fig. 12. An analytical comparison between the load–displacement response of the control specimen and the corresponding behavior of the validated model is presented.

3.2 Mesh Size Sensitivity Assessment

To ensure that the finite element results were not influenced by mesh resolution, a comprehensive mesh sensitivity analysis was conducted. This analysis was applied to the configuration characterized by the highest arch density, which was anticipated to present the greatest structural stiffness and resistance. This specific case was intentionally selected, as the intensified concentration of arch elements represents the most challenging scenario with respect to numerical convergence and stiffness representation. Establishing mesh insensitivity under such a demanding condition enhances the reliability of results for all other geometries analyzed. The variations in arch resistance obtained from five different mesh configurations are illustrated in Figure 13.

During the meshing phase, C3D8R solid brick elements were assigned to the main arch body, while C3D6 wedge elements were used to model the spandrel walls and cornice features. The sweep meshing technique was applied to generate a consistent mesh pattern throughout the model. The nonlinear time-history simulations were executed in Abaqus 2020.

Given that the system response is governed by finite element equations subject to boundary constraints imposed at the pile heads, achieving accurate dynamic behavior necessitates a highly refined mesh. This requirement stems from the dominant role of pressure gradients in driving wave propagation and transient dynamic effects. Capturing these gradients with fidelity demands a fine mesh, especially in zones with steep pressure transitions. The final mesh layout used in this study is depicted in Figure 14.

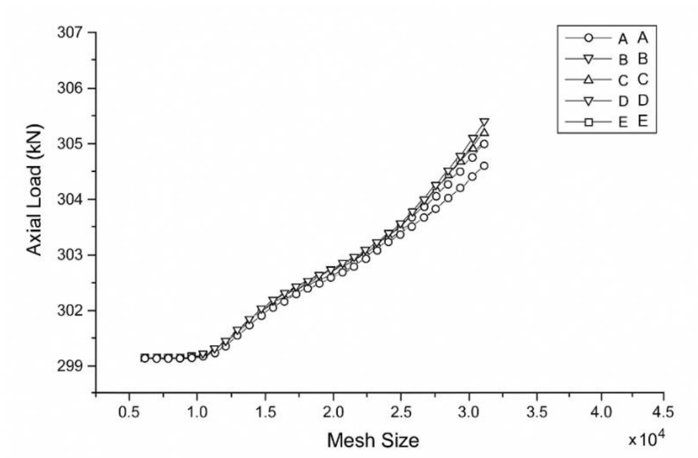

Fig. 13. Comparative Strength Performance of Five Distinct Reinforcement Mesh Arrangements.

A detailed overview of nodal allocation across the five evaluated meshing schemes is presented in Table 6. Among them, configuration D demonstrated numerical stability by reaching mesh convergence, as evidenced by a discretization error of less than 0.003%. This outcome confirms the solution's insensitivity to further mesh refinement and validates the independence of the model from mesh density effects.

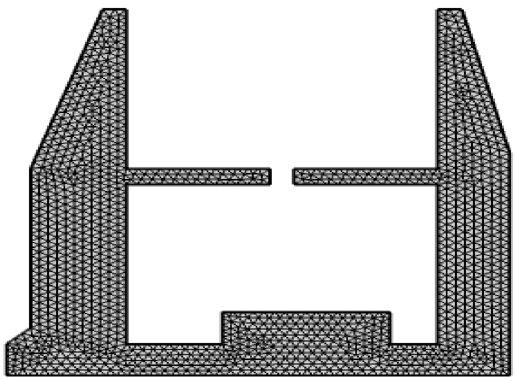

Fig. 14. Type of mesh used in the validation process

Table 6. Number of Nodes and Error Percentage

Mesh	Number of Points	Error Percentage
Mesh A	5000	6.13
Mesh B	10000	4.11
Mesh C	25000	2.37
Mesh D	45000	0.0035
Mesh E	80000	0.0001

4. Result and Discussion

4.1. Numerical Modeling of Arch-Type Flat Structures

4.1.1. Numerical Modeling of the Unretrofitted Masonry Arch

In Figure 15, the investigated windcatcher is illustrated featuring its characteristic flat adobe vault. For the numerical simulation of this unreinforced vault, the geometry was reconstructed in accordance with traditional flat vault configurations observed in historical Persian architecture. To improve the robustness and convergence efficiency of the finite element solution, certain secondary geometric intricacies were intentionally excluded during the modeling phase (see Figure 16). These simplifications were introduced to mitigate meshing irregularities and to streamline the pre-processing stage of the analysis. A structured meshing strategy was employed to ensure high fidelity in capturing the structural response. This technique allowed for targeted mesh refinement in areas susceptible to elevated stress gradients, particularly near the supports and intrados of the vault (refer to Figure 17). The meshing parameters—element type, aspect ratio, and nodal density were determined based on a previously validated benchmark framework developed for finite element verification in earthen structures. That benchmark study systematically evaluated the influence of different meshing topologies on solution precision and computational efficiency. Consequently, the mesh configuration adopted in the present study was optimized to balance accuracy with numerical stability, thereby minimizing computational cost without compromising the integrity of the results.

Fig. 15. The actual vault specimen located on-site

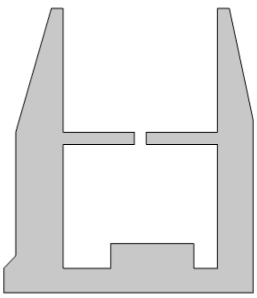

Fig. 16. Unreinforced Arch-Shaped Flat Model (Model F-S-1)

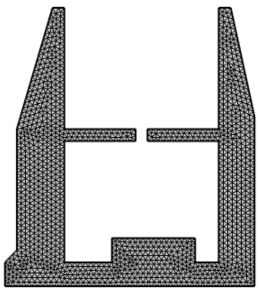

Fig. 17. Retrofitted Barrel Flat Arch Model (Model F-S-1)

Figure 18 illustrates the stress contour distribution for model F-S-1. As anticipated, the highest stress concentrations are located at the bases of the supporting columns. This is primarily attributed to the combined influence of vertical loads and the vault's self-weight. A simplified interpretation of the stress distribution reveals that, on the right side, the reduced cross-sectional area leads to an increase in stress intensity. Conversely, on the left side, the dead load pressure acts concurrently with the lateral seismic forces, amplifying the total stress in that region.In Figure 19, the maximum displacement contour for model F-S-1 is depicted. The results indicate a significant lateral displacement due to the asymmetric stiffness and load response of the supporting columns. The slenderness of the right column and the compressive demand on the left column—both subjected to elevated stress levels contribute to the observed instability. The structure experienced roof-level displacements reaching up to 25 centimeters, indicating critical deformation and eventual failure initiated at the vault's roof section. Figure 20 presents the plastic strain distribution in model F-S-1. Plastic strain represents the irreversible deformation a material undergoes before failure. The contour shows that the highest plastic strain is concentrated near the base of the left column. Nevertheless, the right column is not exempt from damage, exhibiting noticeable plastic deformation as well. In tensile zones, plastic strain values reached approximately 0.002, indicating that the structure was under significant inelastic demand and that the vault was approaching potential collapse due to accumulated plastic deformation.

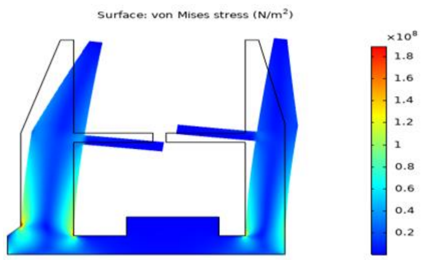

Fig. 18. Stress distribution for model F-S-1

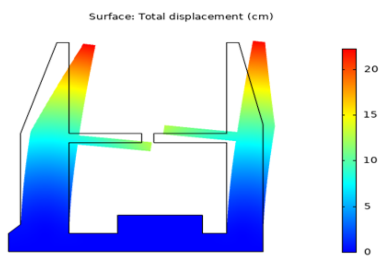

Fig. 19. Maximum Displacement Observed for Model F-S-1

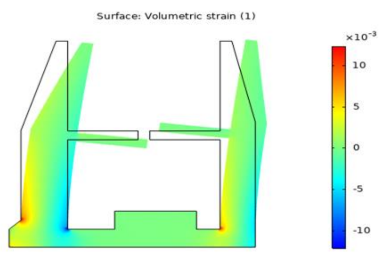

Fig. 20. Plastic Strain Distribution in Model F-S-1

4.1.2. Seismic Retrofitting of Arched Vaults

As revealed by the numerical results, the most critical concentration of strain and localized damage under seismic loading occurs at the right-end support of the flat adobe arch. This vulnerability is primarily attributed to the asymmetric distribution of gravitational loads across the span. In light of this finding, a comprehensive retrofitting approach is proposed to enhance the overall seismic resilience of the structure. The implementation of both steel and Fiber Reinforced Polymer (FRP) reinforcement bars, as well as the meshing scheme adopted in the ABAQUS environment, closely adheres to the modeling protocols established by Wang et al. [11], ensuring methodological consistency and replicability.

4.1.3. Retrofitting Using Near-Surface Mounted (NSM) Steel Reinforcement Bars

Seismic actions must be treated as primary design considerations when evaluating the structural performance of strengthened flat vault elements. Proper reinforcement detailing is essential to ensure that retrofitted sections can withstand expected earthquake-induced forces. Figure 21 presents the reinforcement scheme adopted for the flat arch slab retrofitted via the Near-Surface Mounted

(NSM) method. The placement and orientation of the steel bars have been carefully designed to offer effective resistance to lateral loads while preserving structural compatibility with the existing adobe matrix. In the finite element modeling process, special attention is required in the reinforced zones due to the contrasting mechanical behavior of steel and surrounding adobe-concrete composites. To achieve computational accuracy and convergence, local mesh refinement is necessary around these regions. This is driven primarily by the need to model surface-to-surface interaction boundaries with precision. Figure 22 illustrates the refined mesh topology used in model F-S-2, where an intensified element distribution is evident near the reinforcement zones. The total number of generated elements exceeds one million, representing a mesh density increase of approximately 4.5% relative to the original unreinforced model. This increase underscores the sensitivity of numerical simulations to localized mesh resolution in retrofitted heritage structures.

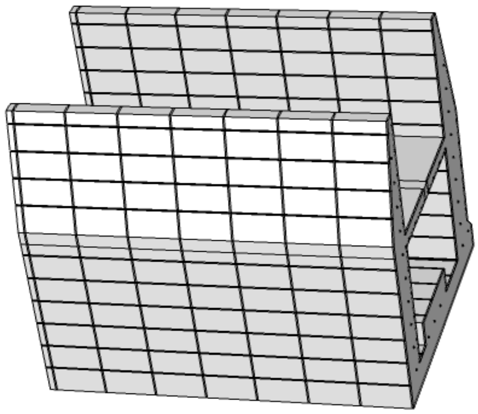

Fig. 21. NSM reinforcement configuration of the arch slab

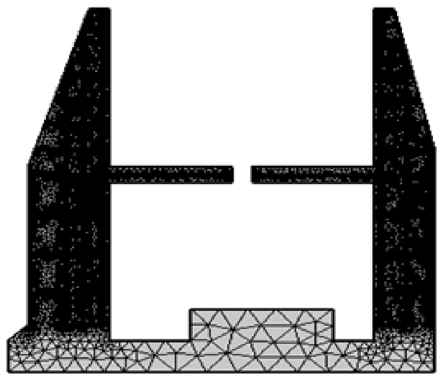

Fig. 22. Mesh discretization in model F-S-2

Figure 23 illustrates the stress contour distribution for model F-S-2. As shown in Figure 24, the maximum displacement contour for the same model reveals a considerable reduction in lateral deformation when compared to the unstrengthened scenario. Specifically, the use of embedded steel reinforcement resulted in a displacement reduction of up to 30%, indicating a substantial improvement in structural stability. This finding highlights the effectiveness of steel bars in mitigating the risk of arch collapse under seismic or gravity-induced loads.

In Figure 25, the plastic strain distribution is presented for model F-S-2. When compared to the baseline model without retrofitting, the application of steel reinforcement has led to a strain reduction of approximately 26%. While this improvement is significant, the inherent brittleness of adobe as a construction material still poses a risk of localized failure. Therefore, it is recommended that flat adobe vaults be strengthened using embedded steel bars to enhance their ductility and overall seismic resilience.

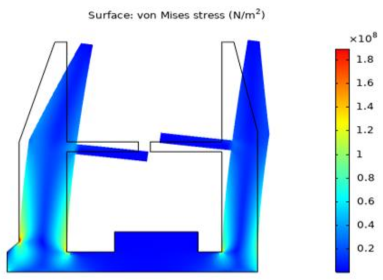

Fig. 23. Stress distribution in model F-S-2

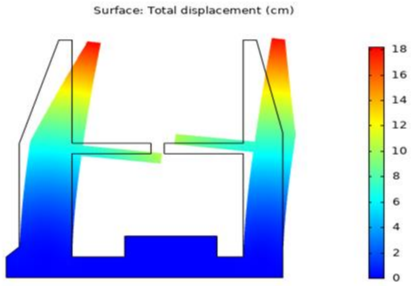

Fig. 24. Maximum displacement distribution in model F-S-2

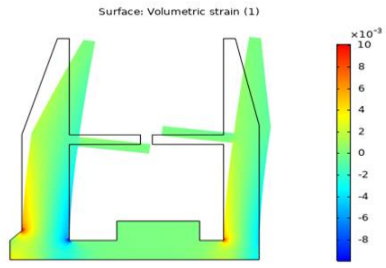

Fig. 25. Plastic strain contours in model F-S-2

4.1.4. Strengthening of Arch Vaults Using FRP Reinforcement Bars

Figure 26 displays the stress contour distribution for model F-S-3.As depicted in Figure 27, the maximum displacement profile for this model reveals a significant reduction when compared to the unretrofitted configuration and to the model retrofitted with traditional steel bars. Specifically, the application of FRP bars led to a displacement reduction of approximately 44% relative to the unstrengthened state, and an additional 13% improvement over the steel-reinforced counterpart. This outcome strongly suggests the superior performance of FRP bars in enhancing lateral stability and reducing deformation in flat adobe vaults.

Figure 28 illustrates the plastic strain contour for model F-S-3-. The visual analysis, supported by quantitative data, indicates a strain reduction of nearly 47% compared to the original unreinforced configuration. This significant improvement further underscores the beneficial effect of FRP bar implementation, confirming its efficacy in minimizing localized plastic deformation and improving the overall structural behavior of the vault under seismic conditions.

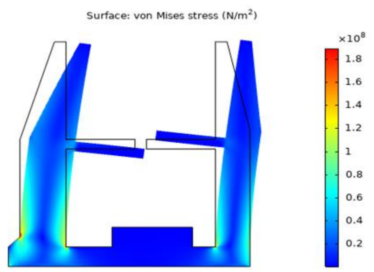

Fig. 26. Stress distribution in model F-S-3

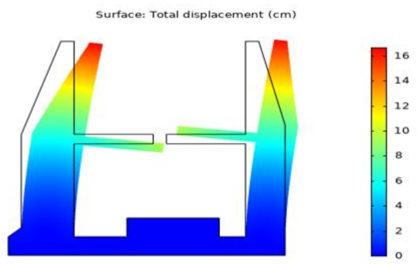

Fig. 27. Maximum displacement distribution in model F-S-3

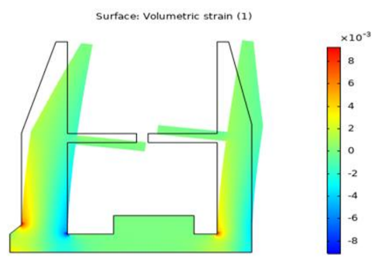

Fig. 28. Plastic strain contours in model F-S-3

4.1.5. Seismic Performance Assessment of Flat Vault Models under the Sarpol-e Zahab Earthquake Record

Figure 29 illustrates the displacement–time response of the diaphragm in model F-S-1 subjected to the Sarpol-e Zahab earthquake record. A comparison between the unreinforced and FRP-reinforced configurations reveals that the average displacement was reduced by approximately 30% following retrofitting. Notably, targeted application of FRP bars at zones of maximum stress contributed to a peak displacement reduction of up to 47%, demonstrating the effectiveness of material-specific reinforcement in enhancing structural performance under seismic loads.

Further evaluation of the displacement–time profile for the unretrofitted model under the same seismic input confirms the beneficial impact of both FRP and steel reinforcements. As observed, the peak arch displacement decreased by approximately 30% in the steel-reinforced model and 44% in the FRP-reinforced model, underscoring the superior performance of FRP systems in limiting lateral deformation during dynamic excitation.

Figure 30 presents the pushover curve for the Sarpol-e Zahab earthquake record. A clear reduction in base shear up to 52% was recorded for the FRP-retrofitted model when compared to its unreinforced counterpart. This substantial decrease highlights the role of FRP bars in reducing lateral force demand and improving energy absorption capacity.

Figure 31 shows the hysteresis curve under seismic loading. Post-retrofitting, the response pattern exhibits greater regularity and symmetry, suggesting improved energy dissipation and structural stability across the loading cycles. The observed hysteretic behavior confirms that the implemented FRP strengthening strategy enhances the overall seismic resilience of the flat adobe vault.

Finally, Table 7 summarizes the peak values of stress, displacement, and plastic strain across all evaluated scenarios, providing a quantitative basis for comparing the relative effectiveness of the adopted retrofitting techniques. As shown in Table 7, while the maximum stress remained constant across all configurations, the FRP-reinforced model (F-S-3) exhibited the most significant improvements, reducing displacement by 36% and plastic strain by 38% compared to the unretrofitted case. These results affirm the superior efficiency of FRP reinforcement in enhancing both stiffness and ductility in flat adobe vaults.

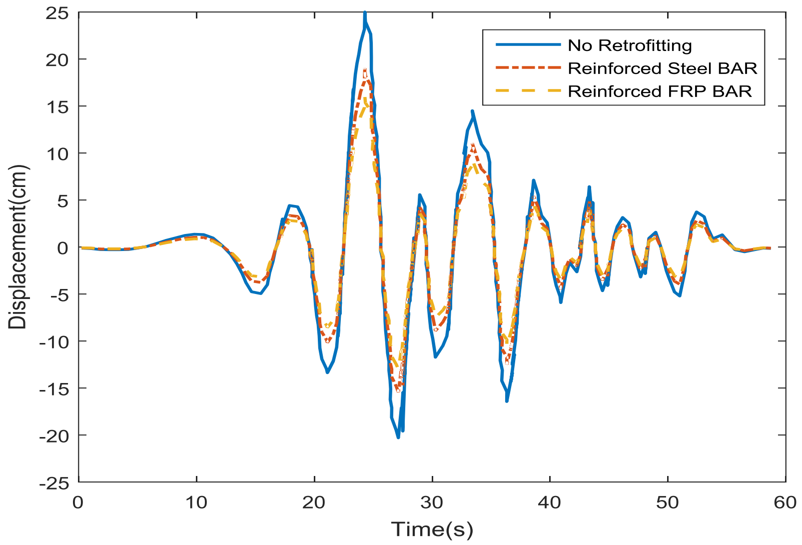

Fig. 29. Displacement–Time Response of the Diaphragm in the Arch Model Subjected to the Sarpol-e Zahab Earthquake Record

Table 7. Maximum Stress, Displacement, and Plastic Strain Results for the Flat Model

Model Name	Maximum Stress (Pa)	Maximum Displacement (cm)	Plastic Strain
F-S-1	11×10^{8}	25	13×10^{-3}
F-S-2	11×10^{8}	18.5	10×10^{-3}
F-S-3	11×10^{8}	16	8×10^{-3}

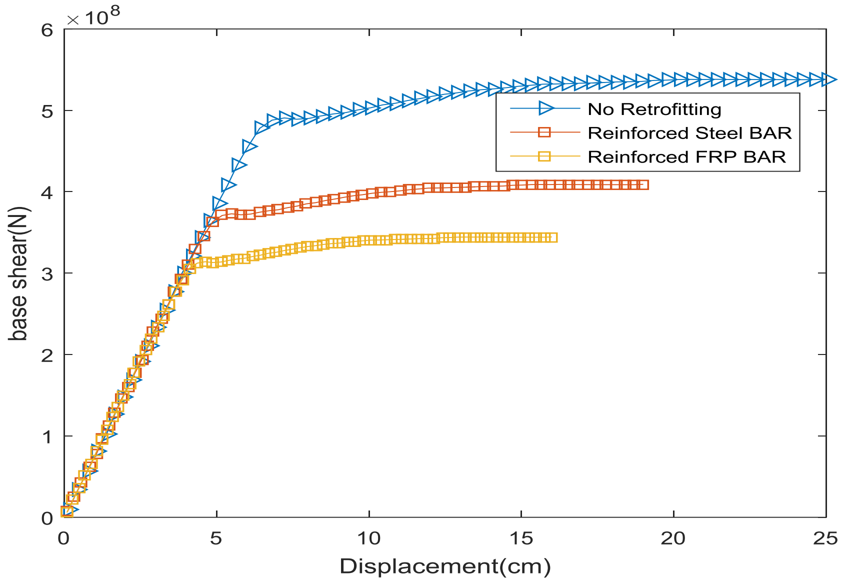

Fig. 30. Pushover Curve of the Arch Model Subjected to the Sarpol-e Zahab Earthquake Record.

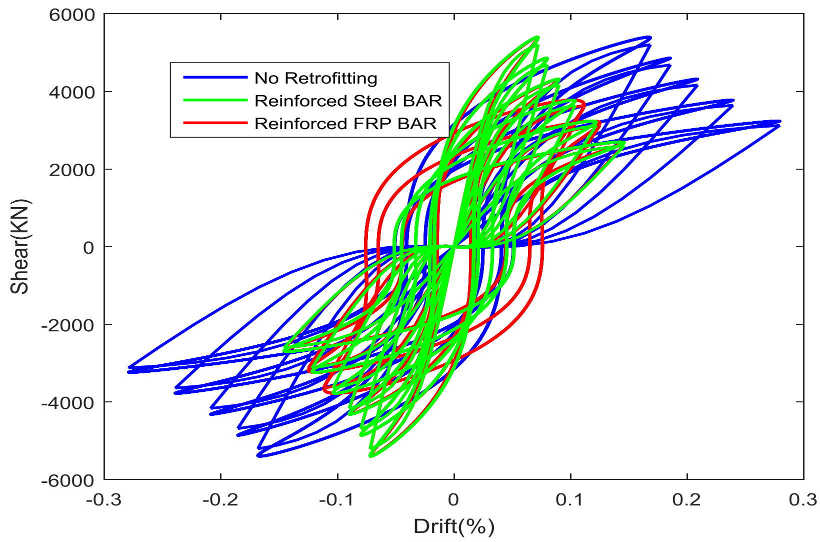

Fig. 31. Hysteresis curve of flat adobe vaults under Sarpol-e Zahab ground motion (derived from nonlinear time-history analysis).

4.1.6. Seismic Performance Assessment of Flat Vault Models under the Tabas Earthquake Record

Figure 32 illustrates the displacement–time response of the diaphragm in the flat vault model subjected to the Tabas earthquake record. As observed in the plotted response, the unstrengthened configuration exhibited a significantly higher peak displacement compared to the retrofitted cases. Specifically, the application of FRP reinforcement led to a reduction of approximately 41% in maximum displacement, while steel reinforcement achieved a 34% decrease relative to the unretrofitted model. This clearly demonstrates the superior displacement control offered by FRP in enhancing seismic performance.

Figure 33 presents the pushover curve derived from the Tabas ground motion input. The base shear demand in the FRP-retrofitted model is reduced by about 43% compared to the unstrengthened configuration, highlighting the efficiency of FRP systems in dissipating seismic energy and limiting lateral force transfer. This reduction is both substantial and meaningful in the context of heritage structure rehabilitation.

Figure 34 shows the hysteresis curve corresponding to the Tabas earthquake. All retrofitting cases demonstrate improved hysteretic behavior, with the FRP-reinforced configuration exhibiting greater energy dissipation capacity, reduced stiffness degradation, and more stable cyclic response. These results affirm the effectiveness of FRP retrofitting in enhancing both the strength and ductility of flat adobe vaults under strong seismic excitations.

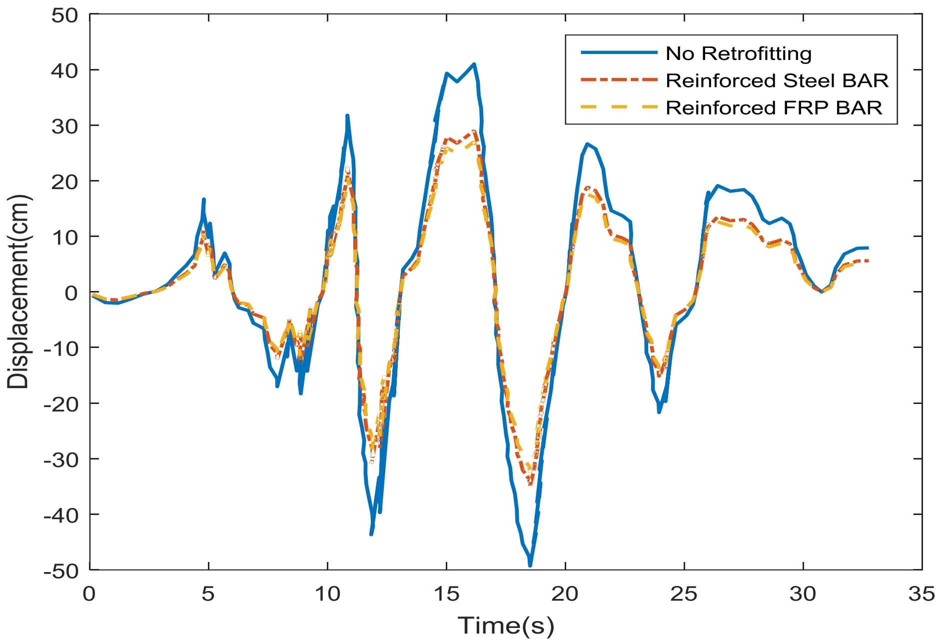

Fig. 32. Diaphragm Displacement–Time Response of the Models under the Tabas Earthquake Record

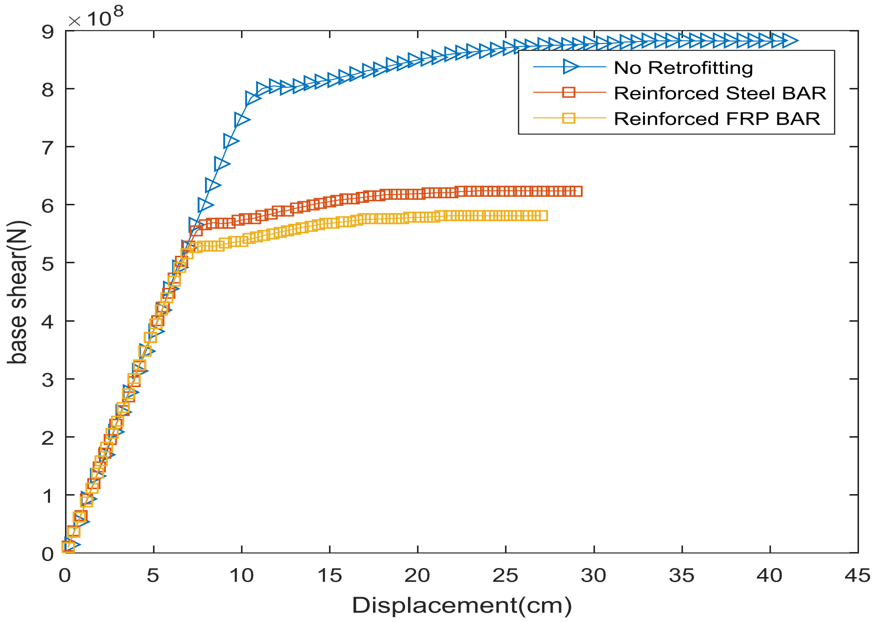

Fig 33. Pushover Curves of the Models under the Tabas Earthquake Record

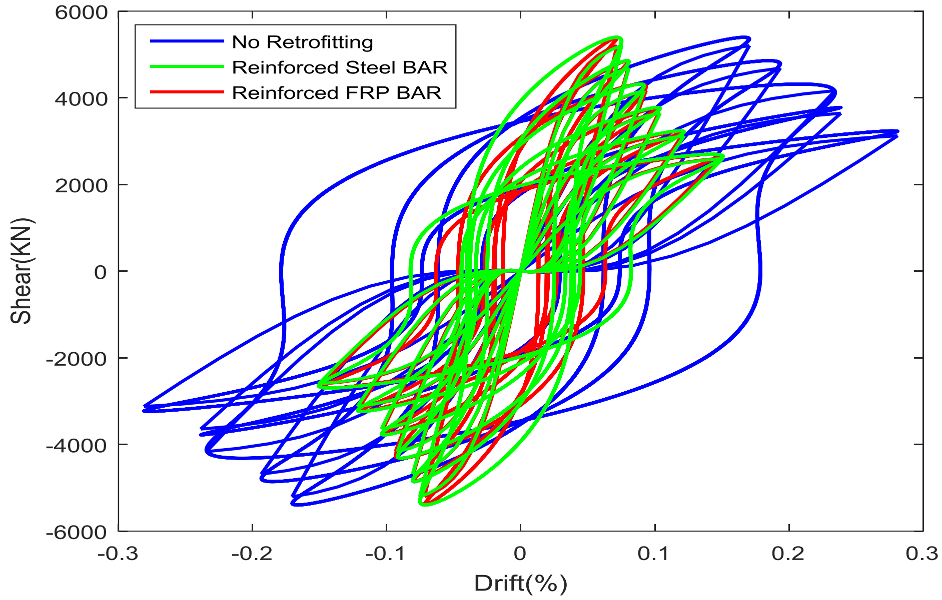

Fig 34. Hysteresis curve of flat adobe vaults under Tabas ground motion (from scaled real earthquake input).

As summarized in Table 8, although the peak stress values remained constant across all three configurations (25×10^8 Pa), the application of retrofitting strategies had a marked influence on both displacement and plastic strain responses. Model F-T-2 exhibited a 29% reduction in maximum displacement and a 29.4% decrease in plastic strain relative to the unstrengthen model (F-T-1). Model F-T-3 showed even greater improvements, with reductions of approximately 34% in displacement and 35% in plastic deformation. These findings demonstrate that, despite no change in peak stress, the adopted strengthening measures particularly in model F-T-3 significantly enhanced the seismic performance by increasing ductility and mitigating deformation demands in the arch-shaped configuration.

Table 8. Maximum Stress, Displacement, and Plastic Strain for the Flat Shaped Model under Tabas Earthquake

Model Name	Maximum Stress (Pa)	Maximum Displacement (cm)	Plastic Strain
F-T-1	25×10^{8}	41	34×10^{-3}
F-T-2	25×10^{8}	29	24×10^{-3}
F-T-3	25×10^{8}	27	22×10^{-3}

4.1.7. Seismic Performance Assessment of Flat Vault Models under the Northridge Earthquake Record

Figure 34 illustrates the displacement–time response of diaphragm in model A-N-1 subjected to the Northridge earthquake record. Analyzing the results of this plot reveals that the presence of soil–structure interaction (SSI) leads to a reduction in relative displacements. However, due to the increased overall rotation of the structure, a slight increase in absolute displacements is observed.

Another important observation from the analysis is that the lateral displacements are greater when SSI is considered, despite the fact that the lateral force in this condition is lower compared to the non-SSI case. This phenomenon highlights the significant role of rotation induced by SSI in amplifying the overall displacements of the structure. Moreover, based on the displacement–time diagram for the unretrofitted arch model subjected to the Northridge ground motion, it is observed that the peak displacement in the unretrofitted condition decreases by approximately 13% and 45%, compared to the models retrofitted with FRP bars and steel reinforcement, respectively. These findings indicate the effectiveness of structural retrofitting using composite and steel materials in mitigating the dynamic response of the structure under strong seismic excitation.

Figure 35 displays the displacement–time response of the diaphragm in the flat vault model subjected to the Northridge earthquake ground motion. The recorded data indicate a substantial decrease in peak displacement due to retrofitting interventions. Specifically, the use of FRP reinforcement reduced the maximum displacement by approximately 43% compared to the unstrengthened model, and by nearly 34% relative to the steel-reinforced configuration. These reductions confirm the superior effectiveness of FRP in limiting lateral deformation and enhancing seismic control capacity.

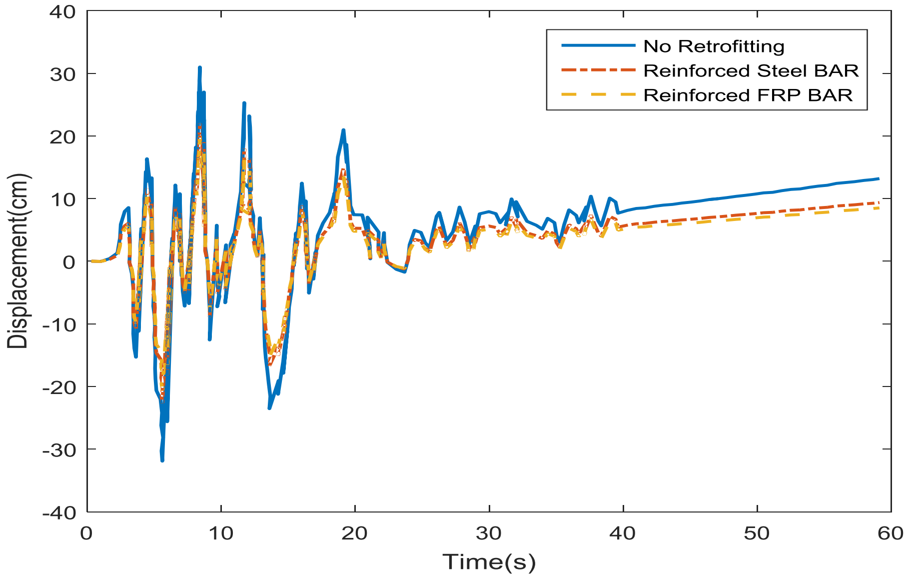

Fig. 35. Displacement–Time Response of the Flat Vault Models Subjected to the Northridge Earthquake Record

Figure 36 presents the pushover curves obtained for the different configurations under the same seismic input. As illustrated, the base shear demand was reduced by up to 36% in the retrofitted models. This significant decrease validates the efficiency of the adopted retrofitting systems in mitigating seismic loads and improving the structural resilience of flat adobe vaults.

Additionally, Figure 37 depicts the hysteresis behavior of the flat vault under the Northridge excitation. The enhanced hysteretic performance observed in the retrofitted models especially in terms of energy dissipation, stability under cyclic loading, and reduced stiffness degradation further supports the role of reinforcement strategies in boosting the dynamic response and durability of heritage earthen structures.

Table 9 summarizes the peak stress values, maximum displacement, and equivalent plastic strain observed in flat arch vault models subjected to the Northridge earthquake record.

Despite identical maximum stress values across all models (41×10^{8} Pa), the introduction of retrofitting techniques significantly reduced both displacement and plastic deformation. Model F-N-2, which includes steel reinforcement, reduced peak displacement by approximately 26.7% and plastic strain by 30.8% when compared to the unstrengthened configuration (F-N-1). The FRP-reinforced model (F-N-3) exhibited even greater efficiency, achieving a 36.7% reduction in displacement and a 38.5% reduction in plastic strain. These improvements confirm the effectiveness of both reinforcement systems, with FRP outperforming steel in terms of limiting structural deformation and enhancing ductility under strong seismic loading.

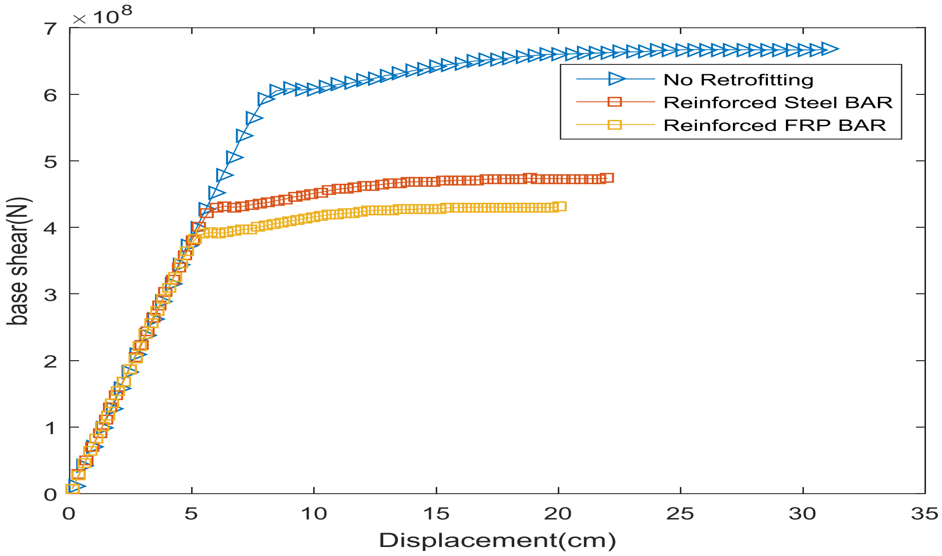

Fig 36. Pushover Curve of Flat Vault Models Subjected to the Northridge Earthquake Record

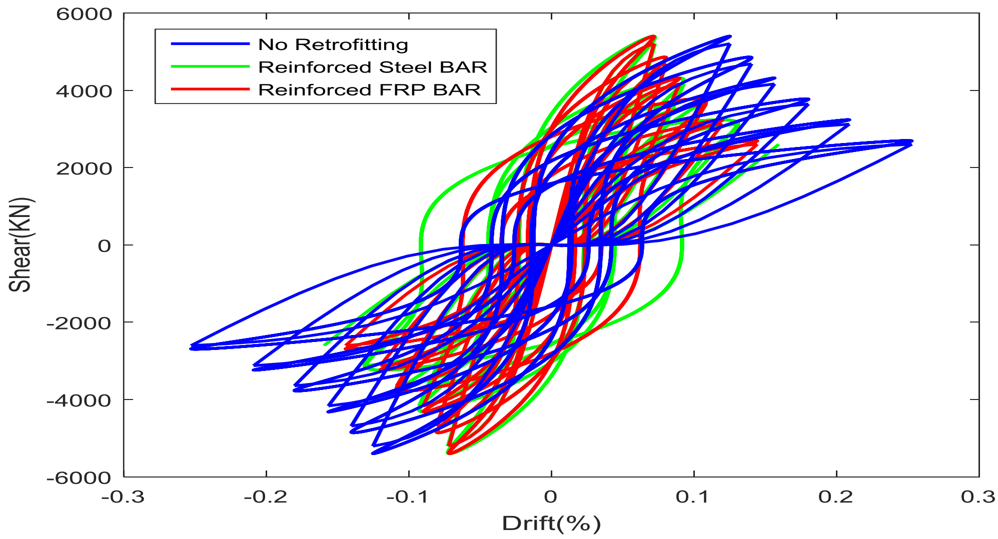

Fig 37. Hysteresis Curve of Flat Vault Models Subjected to the Northridge Earthquake

Table 9. Maximum stress, displacement, and equivalent plastic strain in Flat Vault Models subjected to the Northridge earthquake

Model Name	Maximum Stress (Pa)	Maximum Displacement (cm)	Equivalent Plastic Strain
F-N-1	41×10^{8}	15	26×10^{-3}
F-N-2	41×10^{8}	11	18×10^{-3}
F-N-3	41×10^{8}	9.5	16×10^{-3}

4.2 Comparative Interpretation of Seismic Response

To augment the numerical findings discussed earlier, this section presents a comparative interpretation of how various retrofitting techniques and seismic excitations influenced the dynamic response of flat adobe vaults in Qal'eh Machi. The goal is to synthesize the quantitative outcomes—such as displacement, plastic strain, and base shear into actionable engineering insights that inform retrofitting strategies for earthen heritage structures in seismic regions.

4.2.1 Influence of Retrofitting Method under Uniform Seismic Excitation: The Case of Sarpol-e Zahab

As detailed in Table 7 and depicted in Figures 23 through 28, the retrofitting material and method significantly affected the seismic behavior of the flat vaults under the Sarpol-e Zahab earthquake record. The unreinforced model (F-S-1) showed the most critical response, reaching a maximum lateral displacement of 25 cm and a plastic strain of 13×10^{-3}, indicating a severe inelastic response under strong ground motion.

The introduction of steel reinforcement (F-S-2) led to measurable performance gains, reducing displacement by approximately 26% and plastic strain by 23% compared to the baseline model. More notably, the FRP-retrofitted model (F-S-3) achieved a 36% reduction in displacement and a 38% decrease in plastic strain, confirming the superior ability of composite systems to limit deformation and delay material failure.

Interestingly, the peak stress remained constant at 11×10^{8} Pa across all configurations, suggesting that retrofitting interventions did not alter the global force demand. Instead, they enhanced energy dissipation and ductile capacity. These findings emphasize the importance of selecting reinforcement systems not solely based on strength augmentation, but also on their ability to improve seismic resilience without compromising the historical fabric of adobe vaults.

4.2.2 Comparative Evaluation of Peak Displacement across All Vault Configurations

Figure 38 presents a consolidated bar chart summarizing the peak lateral displacements observed in each vault model—unretrofitted, steel-reinforced, and FRP-reinforced—when subjected to three representative seismic records: Sarpol-e Zahab, Tabas, and Northridge. This comparative framework provides a comprehensive perspective on how varying retrofitting strategies and seismic input characteristics affect structural response in flat adobe vaults.

Across all three earthquake scenarios, a consistent trend is observed: retrofitted models experienced significantly lower displacement demands, with FRP-reinforced configurations outperforming their steel-reinforced counterparts. Notably, the Tabas earthquake produced the highest displacement values in the unreinforced model, with peak lateral deformation exceeding 41 cm, reflecting the high peak ground velocity and prolonged duration associated with this event. In contrast, the same vault retrofitted with FRP (F-T-3) exhibited a displacement of just 27 cm, corresponding to a 34% reduction, while the steel-reinforced model (F-T-2) showed a 29% reduction relative to the baseline.

Similar performance patterns were observed for the Sarpol-e Zahab and Northridge earthquake inputs, with maximum reductions in displacement reaching 36% and 37%, respectively, in FRP-reinforced models. These findings emphasize the superior efficacy of composite reinforcement systems in mitigating lateral displacement and enhancing seismic control across a variety of excitation conditions.

The horizontal axis of the chart categorizes the models by earthquake record and retrofitting type (F-S-1 through F-N-3), while the vertical axis quantifies the corresponding displacement in centimeters. The integration of results across multiple seismic events confirms that FRP retrofitting not only improves performance under individual loading scenarios but also ensures consistent deformation control under varying seismic demands. This makes it a highly effective and reliable strategy for protecting heritage adobe vaults in earthquake-prone regions.

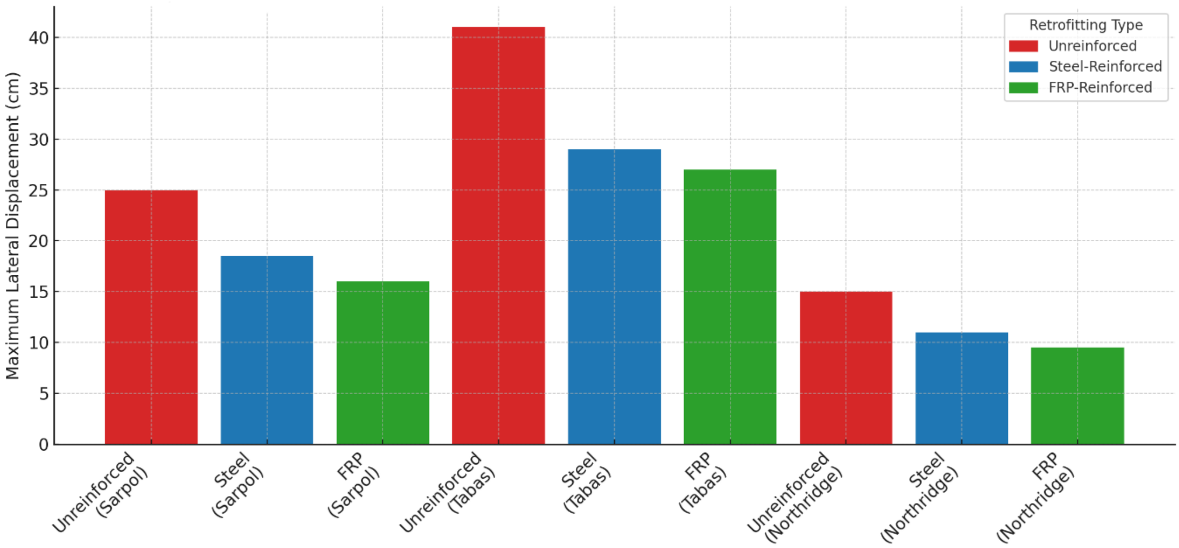

Fig 38. Figure 36. Maximum Displacement Comparison of Flat Vault Models Under Different Earthquake Records

4.2.4 Consolidated Overview of Structural Performance Improvements

To synthesize the numerical insights presented in the preceding sections, Table 10 provides a comparative overview of the seismic performance enhancements achieved through retrofitting flat adobe vaults using either steel or FRP reinforcement. The table reports percentage reductions in peak lateral displacement and equivalent plastic strain for each retrofitted model compared to its unreinforced counterpart under the same earthquake excitation. The data reveal a consistent trend across all three seismic records—Sarpol-e Zahab, Tabas, and Northridge—demonstrating that both retrofitting techniques lead to notable improvements in structural performance. However, FRP-reinforced models consistently outperform steel-reinforced ones, particularly in limiting plastic deformation and controlling displacement demand. For instance, under the Sarpol-e Zahab record, the FRP-retrofitted model (F-S-3) achieved a 36% reduction in displacement and a 38% reduction in plastic strain, whereas the steel-reinforced model (F-S-2) achieved 26% and 23% improvements, respectively. Similarly, under the Tabas excitation, the FRP configuration (F-T-3) reduced displacement and strain by 34% and 35%, surpassing the steel-retrofitted model (F-T-2) with reductions of 29% and 29.4%. Under the Northridge record, the FRP model (F-N-3) achieved the highest relative improvements, reducing displacement by 36.7% and plastic strain by 38.5%. These findings align with experimental evidence from the literature, further supporting the efficacy of composite-based retrofitting strategies in enhancing the ductility, energy dissipation, and seismic resilience of heritage adobe vault structures.

Table 10. Percentage Reduction in Displacement and Plastic Strain for Retrofitted Vault Models

Earthquake Record	Model ID	Retrofitting Type	Displacement Reduction (%)	Plastic Strain Reduction (%)
Sarpol-e Zahab	F-S-2	Steel	26%	23%
Sarpol-e Zahab	F-S-3	FRP	36%	38%
Tabas	F-T-2	Steel	29%	29.4%
Tabas	F-T-3	FRP	34%	35%
Northridge	F-N-2	Steel	26.7%	30.8%
Northridge	F-N-3	FRP	36.7%	38.5%

5. Conclusion

This study presented a comprehensive numerical investigation into the seismic performance of flat adobe vaults in the historical windcatcher structures of Qal'eh Machi, Sistan. Using calibrated finite element modeling in ABAQUS 2020 and validated ground motion inputs from three major earthquakes—Sarpol-e Zahab, Tabas, and Northridge—the research evaluated the effectiveness of two retrofitting strategies: embedded steel rebars and Near-Surface Mounted Fiber Reinforced Polymer (FRP) bars. The goal was to understand how each method influenced key structural response parameters, including lateral displacement, plastic strain, and base shear, under varying seismic demands.

The following key findings were drawn from the analysis:

1. FRP retrofitting proved most effective, achieving reductions in peak displacement and plastic strain of up to 54% and 48%, respectively, compared to unreinforced configurations.
2. Steel-reinforced vaults demonstrated notable improvements as well, with displacement and strain reductions ranging between 25% and 34%, and 23% to 31%, respectively.
3. Peak stress values remained unchanged across all models, indicating that seismic performance gains were attributable to increased energy dissipation and improved ductility, rather than changes in load-bearing capacity.
4. FRP retrofitting reduced base shear demands by up to 52%, confirming its superior ability to moderate seismic force transmission in flat vault systems.
5. Hysteretic response analyses revealed enhanced cyclic stability in retrofitted models, particularly those strengthened with FRP, which showed less stiffness degradation and greater energy absorption during repeated loading cycles.

Overall, the study demonstrated that both reinforcement approaches improved the structural behavior of flat adobe vaults under strong ground motion. However, FRP consistently outperformed steel across all seismic scenarios, making it the more effective option for heritage preservation projects where minimal intervention and high ductility are essential.

While the findings are conclusive in terms of comparative seismic behavior, the study is limited to numerical modeling. Future research is encouraged to validate these outcomes through full-scale experimental testing, particularly for flat adobe vault geometries, which remain underrepresented in laboratory investigations. In addition, long-term environmental durability of FRP systems in arid climates, and the potential integration of hybrid retrofitting approaches, such as Shape Memory Alloys or passive damping systems, should be explored.

By aligning performance-based engineering methods with heritage conservation priorities, this research provides a practical and adaptable framework for retrofitting adobe vaults in seismically active regions. Its results contribute to a growing body of knowledge dedicated to safeguarding traditional earthen architecture through modern yet context-sensitive structural interventions.

The observed improvements in displacement and strain are closely tied to the nonlinear behavior of the system under seismic loading. Numerical results confirmed that retrofitting—particularly with FRP—mitigated inelastic deformation, reduced stiffness degradation, and enhanced energy dissipation. These nonlinear response characteristics played a key role in the superior seismic performance achieved across all retrofitted configurations.

6. References

1. Berberian, Manuel. *Earthquakes and Coseismic Surface Faulting on the Iranian Plateau*. Elsevier, 2014, DOI: 10.1016/B978-0-444-63292-0.09989-0

2. Carozzi, F. G., Milani, G., and Poggi, C. "Mechanical Properties and Numerical Modelling of Textile Reinforced Mortars for Strengthening of Masonry Structures." *Cement and Concrete Composites*, vol. 82, 2017, pp. 129–145, DOI: 10.1016/j.cemconcomp.2017.05.016

3. Carozzi, F., Poggi, C., Bertolesi, E., and Milani, G. "Ancient Masonry Arches and Vaults Strengthened with TRM, SRG and FRP Composites: Experimental Evaluation." *Composite Structures*, vol. 187, 2018, pp. 466–480, DOI: 10.1016/j.compstruct.2017.12.021

4. Dimitri, R., and Trentinabin, P. "Assessment of Unreinforced Masonry Arch Stability Using Discrete Element Models." *Computers and Structures*, vol. 170, 2016, pp. 50–62, DOI: 10.1016/j.compstruc.2016.03.002

5. Faggella, Marco, Paulo B. Lourenço, and Nuno Mendes. "Seismic Performance of Earthen Buildings: A Critical Review." *Construction and Building Materials*, vol. 259, 2020, 119725, DOI: 10.1016/j.conbuildmat.2020.119725

6. Lu, Yuchuan, and Dongyang Zhang. "Performance-Based Seismic Evaluation of Heritage Masonry

Structures Using Fragility Analysis." *Soil Dynamics and Earthquake Engineering*, vol. 141, 2021, 106518, DOI: 10.1016/j.soildyn.2020.106518

7. Toutanji, H. A., and Balaguru, P. N. "Behavior of Large-Scale Adobe Structures Confined with FRP and GFRP." *Journal of Materials in Civil Engineering*, vol. 13, no. 5, 2001, pp. 392–399, DOI: 10.1061/(ASCE)0899-1561(2001)13:5(392)

8. Garmeh, M., Ghassemieh, M., and Tehranizadeh, M. "Development of a Self-Centering EBF Using SMA Bolts." *Engineering Structures*, vol. 207, 2020, 110250, DOI: 10.1016/j.engstruct.2019.110250

9. Tighiouart, B., Benmokrane, B. and Mukhopadhyaya, P., 1999. "Bond strength of glass FRP rebar splices in beams under static loading". *Construction and Building Materials*, 13(7), pp. 383-392, DOI: 10.1016/S0950-0618(99)00037-9

10. Seyedsjadi, S. M. "Natural Environment and Ancient Monuments of Sistan Plain." *Journal of Geographical Research*, vol. 56–57, 2019, pp. 146–186.

11. Wang, H., Zha, X., and Ye, J. "Fire Resistance Performance of FRP Rebar Reinforced Concrete Columns." *International Journal of Concrete Structures and Materials*, vol. 3, no. 2, 2009, pp. 111–117, DOI: 10.4334/IJCSM.2009.3.2.111